The 0-1 Test for Chaos: A review

Georg A. Gottwald and Ian Melbourne

Abstract We review here theoretical as well as practical aspects of the 0-1 test for chaos for deterministic dynamical systems. The test is designed to distinguish between regular, i.e. periodic or quasi-periodic, dynamics and chaotic dynamics. It works directly with the time series and does not require any phase space reconstruction. This makes the test suitable for the analysis of discrete maps, ordinary differential equations, delay differential equations, partial differential equations and real world time series. To illustrate the range of applicability we apply the test to examples of discrete dynamics such as the logistic map, Pomeau-Manneville intermittency maps with both summable and nonsummable autocorrelation functions, and the Hamiltonian standard map exhibiting weak chaos. We also consider examples of continuous time dynamics such as the Lorenz-96 system and a driven and damped nonlinear Schrödinger equation. Finally, we show the applicability of the 0-1 test for time series contaminated with noise as found in real world applications.

1 Introduction

The 0-1 test for chaos was developed in a series of papers [19, 20, 22] to distinguish between regular and chaotic dynamics in deterministic dynamical systems. Rather than requiring phase space reconstruction which is necessary to apply standard Lyapunov exponent methods to the analysis of discretely sampled data, the test works directly with the time series and does not involve any preprocessing of the data. The test requires only a minimal computational effort independent of the dimension of

Georg A. Gottwald

School of Mathematics & Statistics, The University of Sydney, 2006 Sydney NSW, Australia, e-mail: georg.gottwald@sydney.edu.au

Ian Melbourne

Mathematics Institute, University of Warwick, Coventry CV4 7AL, U.K. e-mail: I.Melbourne@warwick.ac.uk

the underlying dynamical system under investigation.

The test has found applications in a wide range of fields. Besides general studies of dissipative [35, 12, 67] and Hamiltonian [72] dynamical systems and multi-agent systems [39], the test has found its way into as disparate areas as engineering [42, 43, 55], electronics [65], finance and economics [36, 69, 68, 70, 38, 37, 28], geophysical applications [48, 47, 60, 7], hydrology [32, 40], epidemology [50, 8, 9] and traffic dynamics [34]. In particular its application to non-smooth processes [42, 43, 2], to systems with fractional derivatives and delays [3, 71, 5], and to non-chaotic strange attractors [18] are notable as those are not amenable to standard methods employing Lyapunov exponents. The test has also been used to analyse systems with non-local operators in integro-differential equations [62] and integro-partial differential equations [10]. Moreover, it has been used to analyse experimental data and observations [13, 33, 34, 38, 37].

The remainder is organised as follows. In Section 2 we briefly describe the test. The algorithm is then presented in Section 3 where we discuss several implementations of the test. The theoretical underpinning of our test is explained in Section 4. This is followed by numerical results in Section 5 illustrating the efficiency of our test to deal with intermittent maps, chaos in thin separatrix layers in Hamiltonian systems, partial differential equations and data contaminated by observational noise. We conclude with a summary in Section 6.

2 Description of the test

The input of the test is a one-dimensional time series $\phi(n)$ for $n = 1, 2, \ldots$ We use the data $\phi(n)$ to drive the 2-dimensional system

$$
\begin{aligned}
p(n+1) &= p(n) + \phi(n)\cos cn, \\
q(n+1) &= q(n) + \phi(n)\sin cn,
\end{aligned}
\tag{1}
$$

where $c \in (0, 2\pi)$ is fixed. Define the (time-averaged) mean square displacement

$$
M(n) = \lim_{N\to\infty} \frac{1}{N} \sum_{j=1}^{N} \left([p(j+n) - p(j)]^2 + [q(j+n) - q(j)]^2 \right), \quad n = 1, 2, 3, \ldots
$$

and its growth rate

$$
K = \lim_{n\to\infty} \frac{\log M(n)}{\log n}.
$$

Under general conditions, the limits $M(n)$ and K can be shown to exist, and K takes either the value $K = 0$ signifying regular dynamics or the value $K = 1$ signi-

fying chaotic dynamics.

A brief explanation of the rationale behind the test is as follows. (The mathematics is described more carefully in Section 4.) In the regular case (periodic or quasiperiodic dynamics) the trajectories for the system (1) are typically bounded, whereas in the chaotic case the trajectories for (1) typically behave approximately like a two-dimensional Brownian motion with zero drift and hence evolve diffusively (i.e. with growth rate $\sqrt{n}$). A convenient method for distinguishing these growth rates, bounded or diffusive, is via the mean square displacement $M(n)$ which accordingly is either bounded or grows linearly. The diagnostic $K \in \{0,1\}$ captures this growth rate.

To summarise, we have the following two scenarios:

Underlying dynamics	Dynamics of $p(n)$ and $q(n)$	$M(n)$	K
regular	bounded	bounded	0
chaotic	diffusive	linear	1

In the following Section we describe the test in more detail focusing on the practical issues in the implementation of the 0-1 test.

3 Description of the algorithm

The test can be readily implemented in a few lines of code. We briefly describe its implementation and refer the reader to [22] for more details. Given a time series $\phi(j)$ for $j = 1, \ldots, N$ we perform the following sequence of steps:

1. For $c \in (0, \pi)$, we solve the system (1) to obtain

$$p_c(n) = \sum_{j=1}^{n} \phi(j) \cos jc, \quad q_c(n) = \sum_{j=1}^{n} \phi(j) \sin jc \qquad (2)$$

for $n = 1, 2, \ldots, N$. Typical plots of p and q for regular and chaotic dynamics are given in Figure 1 which clearly illustrates the bounded motion of p and q for underlying regular dynamics and asymptotic Brownian motion for underlying chaotic dynamics.

2. To analyse the diffusive (or non-diffusive) behaviour of p_c and q_c we compute

$$M_c(n) = \frac{1}{N} \sum_{j=1}^{N} \left([p_c(j+n) - p_c(j)]^2 + [q_c(j+n) - q_c(j)]^2 \right). \qquad (3)$$

To assure the limit $N \to \infty$ we require $n \ll N$. Hence we calculate $M_c(n)$ only for $n \leq N_0$ where $N_0 \ll N$. In practice we find that N_0 should not be chosen much
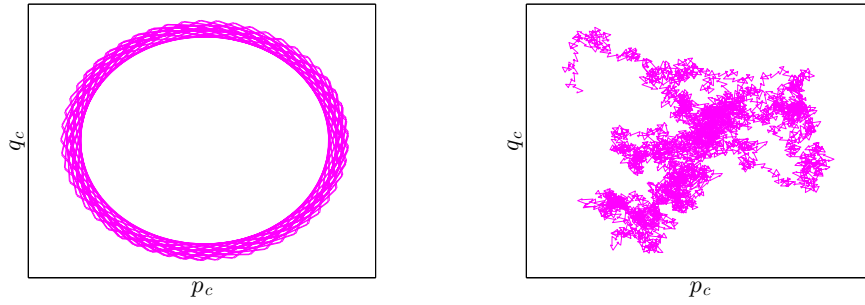
Fig. 1 Plot of p versus q for the logistic map $x_{n+1} = \mu x_n(1-x_n)$. Left: Regular dynamics at $\mu = 3.55$; Right: Chaotic dynamics at $\mu = 3.97$. We used $N = 5000$ data points.

larger than $N/10$.

In [23] a modified mean square displacement

$$D_c(n) = M_c(n) - V_{\mathrm{osc}}(c,n) \qquad (4)$$

was derived which exhibits the same asymptotic growth rate as $M_c(n)$ but with better convergence properties. The correction term

$$V_{\mathrm{osc}}(c,n) = (E\phi)^2 \frac{1 - \cos nc}{1 - \cos c}$$

is readily estimated from the time average of the observable

$$E\phi = \lim_{N \to \infty} \frac{1}{N} \sum_{j=1}^{N} \phi(j) \,.$$

Note that the asymptotic growth rates of $M_c(n)$ and $D_c(n)$ are the same.

In Figure 2 we show the two mean square displacements $M_c(n)$ and $D_c(n)$ for the logistic map $x_{n+1} = \mu x_n(1-x_n)$ with $\mu = 3.97$ (which corresponds to chaotic dynamics) and an arbitrary value of $c = 0.9$. The subtraction of the oscillatory term $V_{\mathrm{osc}}(c,n)$ clearly regularizes the linear behaviour of $M_c(n)$. This allows for a much better determination of the asymptotic growth rate K_c of the mean square displacement which is described in the next step.

3. The contrasting behaviour of the translation variables p_c and q_c as seen in Figure 1 can be distinguished by the asymptotic growth rate K_c of the mean square displacement (or of the modified mean square displacement $D_c(n)$). We present here two different methods to compute K_c, namely the *regression method* and the *correlation method*.
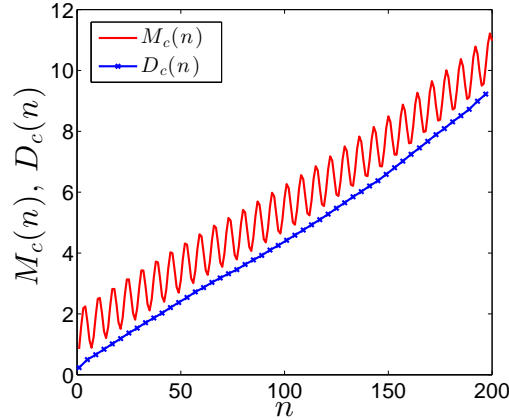
Fig. 2 Plot of the mean square displacement versus n for the logistic map with $\mu = 3.97$ corresponding to chaotic dynamics. We used $N = 2000$ data points and computed $M_c(n)$ and $D_c(n)$ for $n = 1, \ldots, 200$ and an arbitrary value of $c = 0.9$.

Regression method: The regression method consists of linear regression for the log-log plot of the mean square displacement (cf. Figure 2). For the original mean square displacement $M_c(n)$, the asymptotic growth rate K_c is given by the definition

$$K_c = \lim_{n \to \infty} \frac{\log M_c(n)}{\log n} \, .$$

Numerically, K_c is determined by fitting a straight line to the graph of $\log M_c(n)$ versus $\log n$ through minimizing the absolute deviation[1]. It is recommended to minimize the absolute deviation rather than employing the usual least square method as the latter assigns a higher weight to outliers. Outliers are typical of small values of n since the linear behaviour of the mean square displacement is only given asymptotically.

As seen in Figure 2, $D_c(n)$ exhibits far less variance than $M_c(n)$ so it is natural to apply the regression method to $D_c(n)$. However, since $D_c(n)$ may be negative due to the subtraction of the oscillatory term $V_{\mathrm{osc}}(c, n)$, we need to set

$$\tilde{D}_c(n) = D_c(n) + a \min_{1 \le n \le N_0} |D_c(n)| \, ,$$

where $a > 1$ (in the simulations presented here we chose $a = 1.1$) to obtain the asymptotic growth rate

$$K_c = \lim_{n \to \infty} \frac{\log \tilde{D}_c(n)}{\log n} \, .$$

---

[1] One may either use off the shelf routines provided for example in *Numerical Recipes* [61] or build-in routines in MATLAB [49].

Again, K_c can be determined numerically by regression (minimizing the absolute deviation) for the graph of $\log \tilde{D}_c(n)$ versus $\log n$.

Correlation method: In the correlation method, we form vectors $\xi = (1, 2, \ldots, N_0)$ and $\Delta = (D_c(1), D_c(2), \ldots, D_c(N_0))$ (alternatively, $M_c(n)$ could be used instead of $D_c(n)$). Recalling the definition of covariance and variance of given vectors x, y of length q

$$\mathrm{cov}(x, y) = \tfrac{1}{q} \sum_{j=1}^{q} (x(j) - \bar{x})(y(j) - \bar{y}), \quad \text{where} \quad \bar{x} = \tfrac{1}{q} \sum_{j=1}^{q} x(j) ,$$
$$\mathrm{var}(x) = \mathrm{cov}(x, x) ,$$

we define the correlation coefficient

$$K_c = \mathrm{corr}(\xi, \Delta) = \frac{\mathrm{cov}(\xi, \Delta)}{\sqrt{\mathrm{var}(\xi)\mathrm{var}(\Delta)}} \in [-1, 1] .$$

This quantity measures the strength of the correlation of $D_c(n)$ with linear growth. The correlation method greatly outperforms the regression method (see Figures 3 and 4 below), but assumes that the dynamics is such that with probability 1 we have $K_c = 0$ or $K_c = 1$. This is justified for large classes of dynamical systems [23].

4. Steps 1–3 need to be executed for various values of c. In practice, 100 choices of c is sufficient. We then compute the median of these values of K_c to compute the final result $K = \mathrm{median}(K_c)$. The values of c are chosen randomly in the interval $c \in (\pi/5, 4\pi/5)$ to avoid resonances. Resonances occur when the dynamics involves a periodic component with frequency ω implying a term in the Fourier decomposition of the observable ϕ proportional to $\exp(-i\omega k)$. In this case there is a resonance at $c = \omega$ leading to $p_c(n) \sim n$ and $q_c(n) \sim n$ and hence $M_c(n) \sim n^2$ (and $D_c(n) \sim n^2$) implying $K_c = 2$ for the regression method and $K_c \approx 1$ for the correlation method. Note that for $c = 0$ the test would yield a resonance irrespective of the underlying dynamics (which is why this value should be excluded). See [19, 22] for more details on resonances. In Figure 3 we show K_c versus c for the logistic map for regular and chaotic dynamics. Resonances are clearly visible for the periodic case, with $K_c = 2$ for the regression method and $K_c \approx 1$ for the correlation method.

Our test states that a value of $K \approx 0$ indicates regular dynamics, and $K \approx 1$ indicates chaotic dynamics. This is exemplified in Figure 4 where K is shown as a function of the parameter μ of the logistic map.

Remark on finite size problems: There are finite size issues that are inherent to all methods for chaos detection, namely that the length of the time series is sufficiently long to capture the dynamics across the whole of the attractor. Specifically, for the 0-1 test the determination of the mean square displacement requires $n \leq N_0 \ll N$, and the test relies on asymptotic behaviour of the (non)-diffusive behaviour of p and q which for too small time series data length may not yet be dominant. Concerning the latter point it is pertinent to mention that even in cases of time series which are
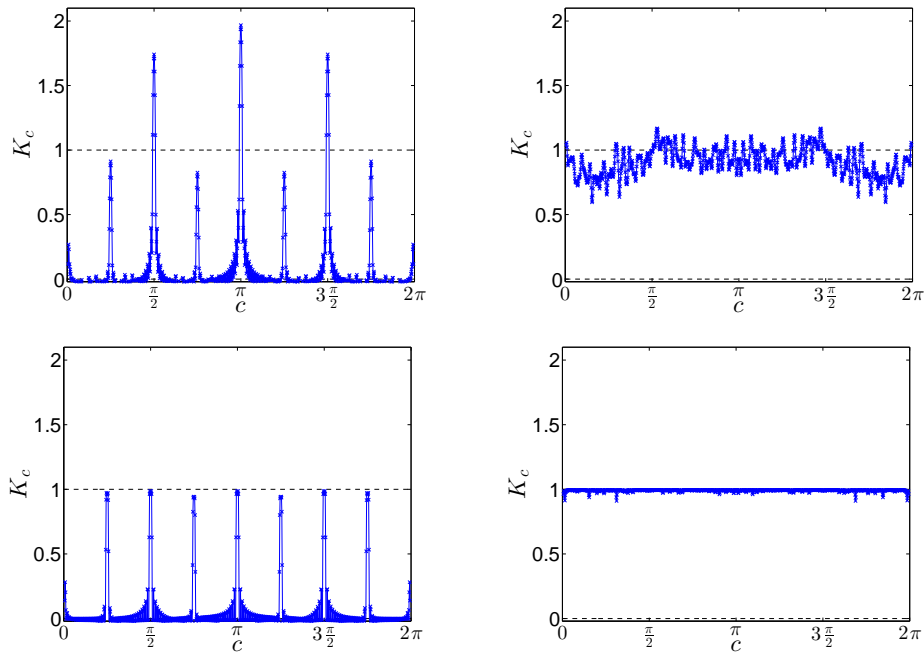
Fig. 3 Plot of K_c versus c for the logistic map calculated using the regression method (top) and correlation method (bottom). We used here $N = 5000$ data points, and 1000 equally spaced values for c. Left: $\mu = 3.55$ corresponding to regular dynamics; Right: $\mu = 3.97$ corresponding to chaotic dynamics.

too short to allow for convergence of K to either 0 or 1, strong indications for the presence or absence of chaos can be found by looking at the behaviour of K with

Fig. 4 Plot of K versus μ for the logistic map with $3.5 \leq \mu \leq 4$ increased in increments of 0.001. We used $N = 2000$ data points. Shown are results when K is calculated via the regression method (dashed line, blue) and when K is calculated via the correlation method (continuous line, red). The horizontal lines indicate the limiting cases $K = 0$ and $K = 1$. We used 100 randomly distributed values of c, and the mean square displacement was determined using $D_c(n)$.
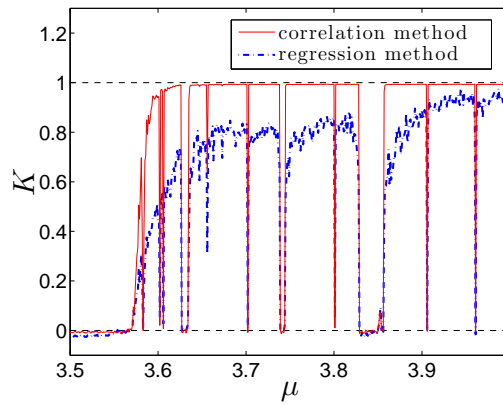
the length of the time series used to determine K. Figure 5 shows typical decreasing/increasing behaviour of K near parameter values of the logistic map at the so called *edge of chaos*, indicating regular or chaotic dynamics, respectively. This was discussed at length in [21, 22].
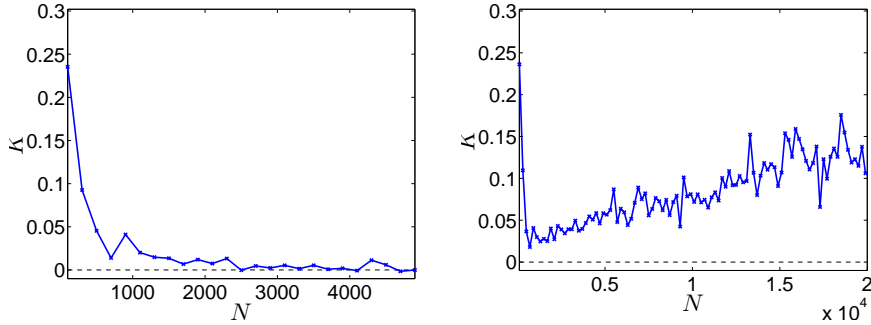
Fig. 5 Plot of K versus the length of the time series N for the logistic map near the edge of chaos. We used 100 randomly distributed values of c, and the mean square displacement was determined using $D_c(n)$ with $N_0 = N/10$, and the correlation method was used to determine K_c. Left: $\mu = 3.569$ corresponding to regular dynamics; Right: $\mu = 3.571$ corresponding to chaotic dynamics.

4 Theoretical framework for the 0-1 test

Systems of the type (1) were studied extensively in [56, 1, 14, 52, 53]. The motivation there was to understand growth rates of trajectories in systems with Euclidean symmetry. A large class of discrete time systems with planar Euclidean symmetry are given by skew product equations of the form

$$
\begin{aligned}
x(n+1) &= f(x(n)), \\
\vartheta(n+1) &= \vartheta(n) + h(x(n)), \\
p(n+1) &= p(n) + \Phi(x(n))\cos(\vartheta(n)) - \Psi(x(n))\sin(\vartheta(n)), \\
q(n+1) &= q(n) + \Phi(x(n))\sin(\vartheta(n)) + \Psi(x(n))\cos(\vartheta(n)).
\end{aligned}
\tag{5}
$$

Here $f : X \to X$ defines the base dynamics (perpendicular to the symmetry variables) while $\vartheta(n)$ represents two-dimensional rotations and $(p(n),q(n))$ represent planar translations. It is assumed that the functions $h, \Phi, \Psi : X \to R$ are smooth. In [56], it was shown that if the dynamics on X is periodic or quasiperiodic, then typically the translation variables $p(n), q(n)$ remain bounded. However, sufficiently chaotic dynamics on X leads to diffusive behaviour in the translation variables. (See [14, 53] for the case of uniformly hyperbolic dynamics, and more recently [25] for nonuniformly hyperbolic dynamics.) Using these results, and computing the growth rate K

of the mean square displacement as described in Section 2, we obtain with probability one the growth rates $K = 0$ and $K = 1$, respectively in these two situations. It is pertinent to stress that the test does not rely in anyway on a possible exponential decay of the auto-correlation function; the test holds for polynomial decay as well and even does not require summability of the auto-correlation function [24, 25] (see also Section 5.1.1). Also it is irrelevant whether the dynamics is mixing. For example, in the case of the logistic map mentioned in Section 5.1, the attractor is almost always a periodic sink or a strongly chaotic attractor consisting of a finite union of intervals permuted cyclically by the dynamics. In both cases, the attractor is mixing up to a finite cycle but is generally nonmixing. More importantly, in the case of continuous time dynamics, it is rarely the case that mixing can be established but the 0-1 test is still valid.

It should be noted that a similar dichotomy holds in the absence of the rotation variables, except that the bounded/diffusive behaviour is superimposed on a linear drift. The rotation symmetry kills off the linear drift [56, 15], rendering the bounded/diffusive dichotomy more readily detectable.

The idea behind the 0-1 test is to adjoin rotation and translation variables ϑ, p, q to a given (but unknown) dynamical system $f : X \to X$ generating data $\phi(n)$, thus producing a system with Euclidean symmetry to which the above theoretical results apply. Note that choosing $h \equiv c$, $\Psi \equiv 0$ and making the identification $\Phi(x(n)) = \phi(n)$ reduces the skew product system (5) to the 2-dimensional system (1) used in the 0-1 test.

The original version of the test [19] used "generic" choices of h so that certain theoretical results of [15] could be applied in justifying the test. The current version is much more effective for noisy data [20] but the original theoretical justification for the test no longer applies. Nevertheless, it transpires that the simplified nature of the equations in (1) enables certain improvements to the theoretical underpinnings for the test, as described in [23]. The structure of the simplified equations means that they are amenable to techniques from Fourier analysis. In particular, there are connections with power spectra as described in the next subsection. In the aforementioned cases of periodic/quasiperiodic dynamics and uniformly/nonuniformly hyperbolic dynamics, we typically obtain $K = 0$ and $K = 1$, respectively. Here "typically" is in the sense of probability one: for almost every choice of c. As mentioned previously, we take the median value of K, computed with 100 randomly chosen choices of c, to circumvent the issue regarding bad choices of c. Moreover, the considerations in [23] lead directly to the modified mean square displacement $D_c(n)$ which we have seen leads to improved results (there is no analogue of this modification for the original test).

4.1 Connection with the power spectrum

Consider a discrete dynamical system $f : X \to X$ with ergodic invariant measure μ. Given a square-integrable observable $v : X \to \mathbf{R}$, the power spectrum S is defined to

be the square of the Fourier amplitudes of $v \circ f^j$ per unit time[2]

$$S(\omega) = \lim_{n \to \infty} \frac{1}{n} \int_X \left| \sum_{j=0}^{n-1} e^{ij\omega} v \circ f^j \right|^2 d\mu, \quad \omega \in [0, 2\pi]. \tag{6}$$

It was proven in [51] that the power spectrum has a broadband nature and is nowhere zero for a large class of dynamical systems, including slowly mixing systems such as Pomeau-Manneville maps provided the auto-correlation function is summable. (For a discussion of recent results in the case of nonsummable autocorrelations, see 5.1.1.)

A simple short calculation shows that

$$S(c) = \lim_{n \to \infty} \frac{1}{n} \int_X |\sum_{j=0}^{n-1} e^{ijc} v \circ f^j|^2 d\mu = \lim_{n \to \infty} \frac{1}{n} M_c(n) , \tag{7}$$

implying that

$$M_c(n) = S(c)n + o(n) . \tag{8}$$

This may give the wrong impression that the 0-1 test for chaos is simply evaluating the power spectrum. From (8) one can only conclude that if the power spectrum is nowhere nonzero ($S(c) \neq 0$ for all c), then the asymptotic growth rate of the mean square displacement becomes $K_c = 1$ for all c. On the other hand, if $S(c) = 0$ for all c, it does not automatically follow that $K_c = 0$ (for example, the $o(n)$ term could be of the form $n/\log(n)$ implying $K_c = 1$). However in [23] it was rigorously proven that for a large class of dynamical systems, the $o(n)$ terms are such that for chaotic dynamics one obtains $K_c = 1$ and for regular dynamics $K_c = 0$.

It is pertinent to mention the computational advantage of the 0-1 test which extracts in a single number K the property of the power spectrum which is relevant for underlying chaotic or regular dynamics, i.e. whether it is everywhere or nowhere nonzero. The test completely bypasses the explicit computation of the power spectrum which would require considerably more data. Moreover, K can be plotted against a parameter of the system as in Figure 4 and the convergence of K can be seen against the number of iterates N as in Figure 5. There do not exist analogous plots for the power spectrum.

5 Numerical examples for the 0-1 test

We now illustrate the applicability of our test to be able to distinguish regular dynamics from chaotic dynamics in discrete and continuous time systems, dissipative and Hamiltonian systems, noise free and noise contaminated data.

---

[2] One may use $e^{2\pi i j\omega/n}$ rather than $e^{ij\omega}$ for a rescaled domain.

5.1 Discrete time systems

One of the simplest families of dynamical systems that exhibits regular and chaotic dynamics is the logistic map $f : [0,1] \to [0,1]$ given by $f(x) = \mu x(1-x)$. Here, $\mu \in [0,4]$ is a parameter. It is well-known that there is a unique attractor for each value of μ and that the basin of attraction is of full measure in $[0,1]$. For almost every value of μ, the attractor is either a periodic orbit or a strongly chaotic attractor. Throughout the earlier Sections, this family of maps was used as an illustrative example for various features of the 0-1 test, see Figures 1, 2, 3, 4 and 5.

We now proceed to explore two further families of discrete time systems.

5.1.1 Pomeau-Manneville map

A prototypical family of maps exhibiting intermittency and weakly chaotic dynamical systems with "sticky" equilibria are Pomeau-Manneville intermittency maps $x_{n+1} = f(x_n)$ with $f : [0,1] \to [0,1]$ given by

$$f(x) = \begin{cases} x(1+2^{\gamma}x^{\gamma}) & 0 \leq x \leq \frac{1}{2} \\ 2x-1 & \frac{1}{2} \leq x \leq 1 \end{cases} \tag{9}$$

where γ is a parameter [59, 44]. For $\gamma \in [0,1)$ there exists a unique absolutely continuous invariant probability measure (SRB measure) ρ. When $\gamma = 0$ the map reduces to the doubling map with exponential decay of correlations. For $\gamma \in (0,1)$ the decay of correlations is polynomial with rate $1/n^{(1/\gamma)-1}$ which is summable for $\gamma < \frac{1}{2}$ and nonsummable for $\gamma \in [\frac{1}{2},1)$ [30]. For $\gamma > 0$ the fixed point at 0 is indifferent ($f'(0) = 1$) and plays the role of the "sticky" regular dynamics leading to laminar behaviour interspersed with intermittent chaotic bursts. This is illustrated in Figure 6, where we show a trajectory of the Pomeau-Manneville map in the strongly chaotic case with $\gamma = 0.2$, where the correlations are summable, and in the intermittent weakly chaotic case with $\gamma = 0.7$, where the correlations are nonsummable.

It is well-known [17] that for such intermittent systems the usual central limit theorem breaks down for $\gamma \in (\frac{1}{2},1)$ leading to fluctuations of Lévy type rather than of Gaussian type. For mathematically rigorous results on this, see [27, 54, 74]. Despite this, our test for chaos is still able to detect chaos in the weakly chaotic case with nonsummable correlations. A proof of this statement is currently work in progress, but the underlying reason, as discussed in related results in [24, 25], is that the anomalous diffusion is suppressed due to the rotation symmetry induced by the presence of c in (2). As a result of this, when the dynamics is trapped near the indifferent fixed point, the dynamics appears regular and therefore leads to bounded dynamics of the translation variables p and q as seen in Figure 7 for $\phi_n = 1 + x_n$. In Figure 8 we show the asymptotic growth rate as a function of γ.
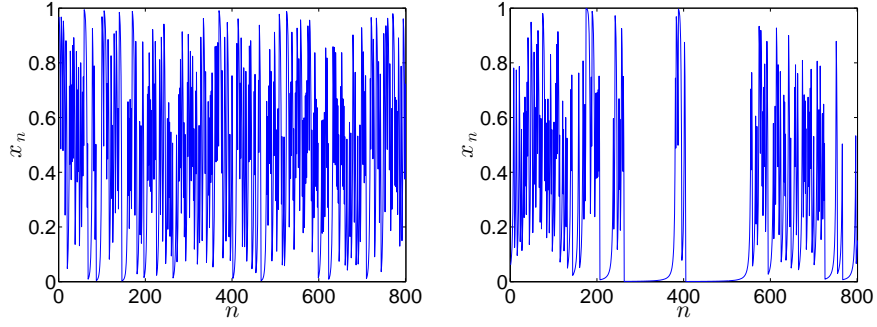
Fig. 6 Time series of the Pomeau-Manneville map (9). Left: Strongly chaotic case with $\gamma = 0.2$. Right: Weakly chaotic case with $\gamma = 0.7$.
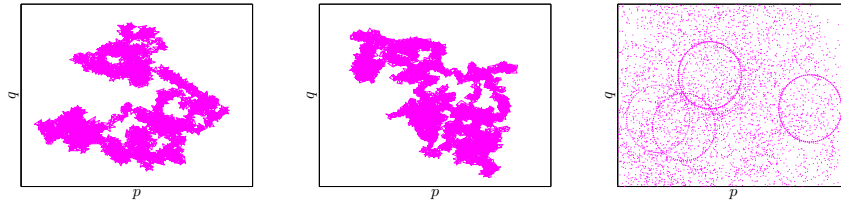
Fig. 7 Typical plots of the translation variables p and q driven by an observable $\phi_n = 1 + x_n$ of the Pomeau-Manneville map (9) for $c = 2.1375$. Left: Strongly chaotic case with $\gamma = 0.2$. Middle: Weakly chaotic case with $\gamma = 0.7$. Right: Zoom for weakly chaotic case with $\gamma = 0.7$ showing the trace of the laminar phases of the Pomeau-Manneville dynamics in form of bounded circles.
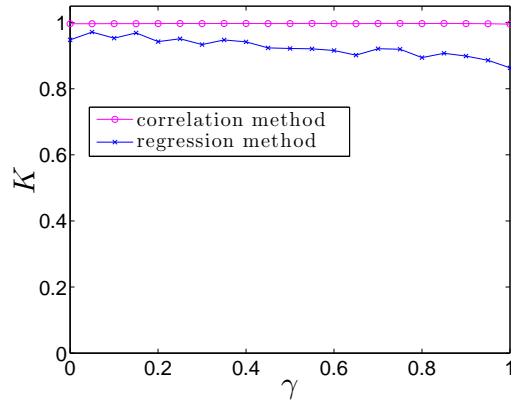
Fig. 8 Plot of K as a function of γ for an observable $\phi_n = 1 + x_n$ of the Pomeau-Manneville map (9), using the regression method (crosses) and the correlation method (circles). We used $N = 10,000$ data points and 100 randomly distributed values of c.
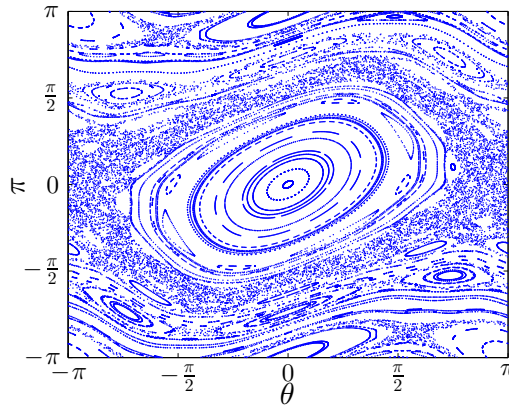

5.1.2 Standard map

We now consider the area-preserving Standard map [6, 41]

$$\pi_{n+1} = \pi_n + \kappa \sin(\theta_n) \tag{10}$$

$$\theta_{n+1} = \theta_n + \pi_{n+1} . \tag{11}$$

Figure 9 shows the trajectories of 100 randomly chosen initial conditions after a transient of $10,000$ iterates for $\kappa = 0.9$. The phase space consists of regular islands embedded in chaotic layers. In contrast, at $\kappa = -0.3$ there is a hyperbolic fixed point at the origin and the asymptotic dynamics occurs in a thin separatrix layer as seen in Figure 10 for 100 randomly chosen initial conditions $\pi_0 \in [0, 0.03]$ and $\theta_0 \in [-0.03, 0.03]$. This thin separatrix layer contains complex structures with many tiny islands embedded within a chaotic sea [29]. This case exhibits *weak* chaos in the sense of [73] with small Lyapunov exponents which may be difficult to distinguish from those corresponding to regular orbits.

In Figures 11 and 12 we show how the 0-1 test is able to detect regular and chaotic orbits, even in the weakly chaotic case. We have chosen $1,000^2$ initial conditions and run them for $10,000$ steps. We used the correlation method and applied it to the modified mean square displacement $D_c(n)$.

**Fig. 9** Standard map (11) exhibiting chaos with $\kappa = 0.9$.

5.2 Continuous time systems

We have so far formulated the 0–1 test for discrete time systems. For continuous time series $\phi(t)$, we obtain a discrete time series $\phi(t_1)$, $\phi(t_2)$, $\phi(t_3)$,... for given discrete times $0 < t_1 < t_2 < t_3 < \cdots$ to which the test for chaos may be applied as in previous sections. The sequence t_j, $j \geq 1$, has to be chosen in a deterministic manner to assure that the time series $\phi(t_j)$ is deterministic. One may choose the t_j as the intersection times with a cross-section. In this case the time series $\phi(t_j)$ corresponds to observing a Poincaré map. A second, perhaps more usual, approach is
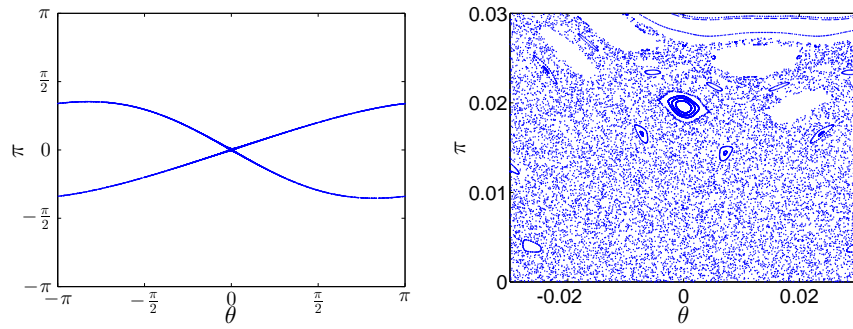
Fig. 10 Standard map (11) exhibiting weak chaos in a small separatrix layer with $\kappa = -0.3$. The right figure is a zoom near the hyperbolic point showing the enlarged stochastic layer.
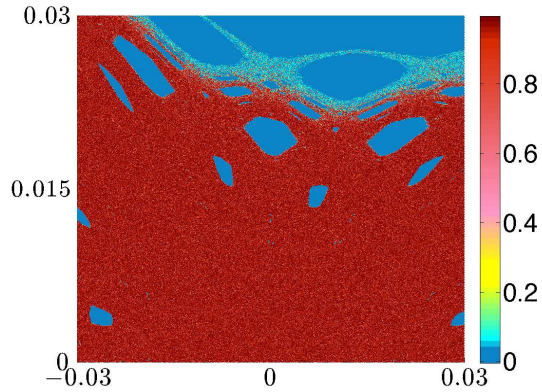

Fig. 11 Contour plot of K for the standard map (11) exhibiting chaos with $\kappa = 0.9$. We used $1,000^2$ equally spaced initial conditions and calculated K via the correlation method from D_c.
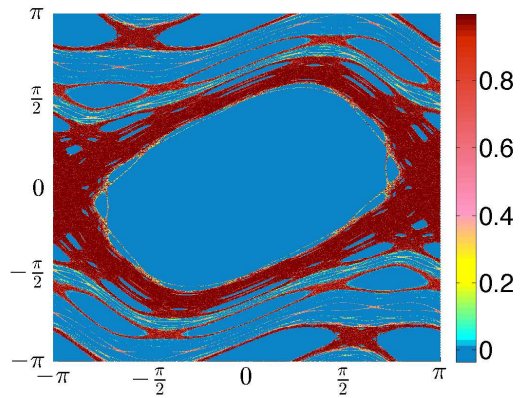
to take $t_j = j\tau_s$ where $\tau_s > 0$ is the sampling time. The time series $\phi(t_j) = \phi(j\tau_s)$ corresponds to observing the "time-τ_s" map associated with the underlying continuous time system. Contrary to the case of observing a Poincaré map, in the latter approach one is faced with a well-known oversampling issue: If τ_s is too small, then the system is *oversampled* and this often leads to incorrect results [22]. Although oversampling is a practical problem for data series of finite size, it should be emphasized that theoretically the test works for all sampling times τ_s in the limit $N \to \infty$. We now present numerical results for an ordinary differential equation and a partial differential equation where care has to be taken to overcome the issue of oversampling for the realistic case of finite data series.

5.2.1 Rössler equations

To illustrate how the issue of oversampling manifests itself in the 0–1 test for chaos and how to overcome it, as proposed in [22], we consider here the 3-dimensional

Fig. 12 Contour plot of K for the standard map (11) exhibiting chaos with $\kappa = -0.3$. We used $1,000^2$ equally spaced initial conditions and calculated K via the correlation method from D_c.
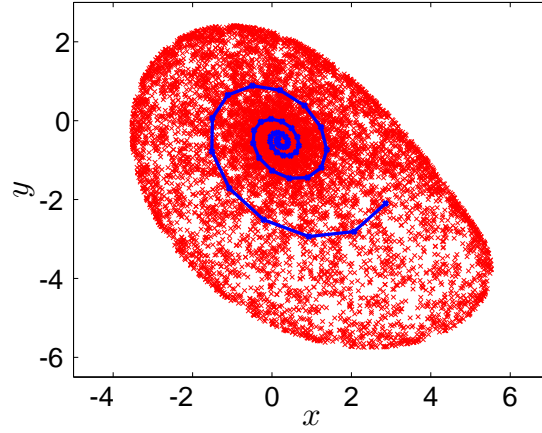
Rössler system [64]

$$\dot{x} = -y - z$$
$$\dot{y} = x + ay$$
$$\dot{z} = b + z(x - d) . \tag{12}$$

For the values $a = 0.432$, $b = 2$ and $d = 4$, the system exhibits chaos with a maximal Lyapunov exponent of about $\lambda_{max} \approx 0.1$ (we use the natural logarithm). We have integrated this system with a fourth-order Runge-Kutta scheme with variable step-size and recorded $100,000$ data points each $\Delta t = 0.01$ (ie. $1,000$ time units) after disregarding a transient behaviour of 50 time units to allow for the dynamics to settle on the attractor. A plot of the dynamic in the x-y-plane is provided in Figure 13.

Figure 14 shows an oversampled and a sufficiently coarsely sampled observable for the Rössler system (12). The finely sampled time series ($\tau_s = 0.05$) yields $K \approx 0$ whereas the coarsely sampled data ($\tau_s = 0.35$) yields $K \approx 1$ already despite using only $1/7$th of the data.

A good choice of the sampling time τ_s can often be obtained by visual inspection as in Figure 14. A more quantitative method is to use the e-folding time of the auto-correlation function or to use the first minimum of the mutual information [16, 31]. For the data depicted in Figure 14 these method yield $\tau_s = 1.15$ and $\tau_s = 1.50$, respectively. However, we observed here, that the smaller sampling time $\tau_s = 0.35$ already yields $K \approx 1$ with the advantage of being a longer data set. In general, the optimal sampling time will depend on the dynamical system and the time series under consideration. We refer the reader to [31] for a discussion on optimal time delays in the context of phase space reconstruction.

In the following we show how the issue of oversampling arises in the 0–1 test. For continuous time systems, the (time-averaged) mean square displacement is defined as

Fig. 13 Phase portrait for the Rössler system (12). The short trajectory segment (blue) was sampled at $\tau_s = 0.5$.
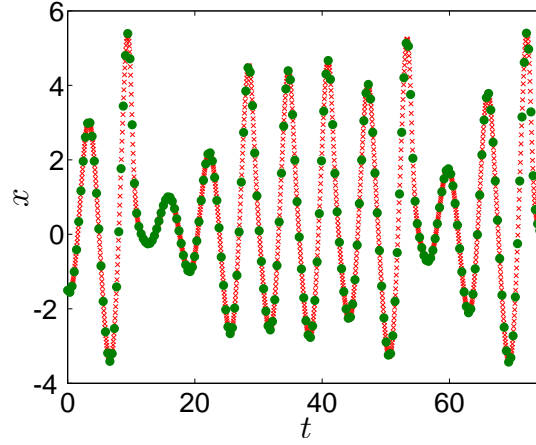
Fig. 14 Plot of the observable $\phi(t) = x(t)$ for the Rössler system (12). The finely sampled data (crosses) are sampled at $\tau_s = 0.05$ time units. The coarsely sampled data (filled circles) are sampled at $\tau_s = 0.35$ time units.

$$M_c(t) = \lim_{T \to \infty} \frac{1}{T} \int_0^T (p(t+\tau) - p(\tau))^2 + (q(t+\tau) - q(\tau))^2 \, d\tau \,,$$

which, for a time series sampled with sample time τ_s, is approximated by

$$M_c(n) = \lim_{N \to \infty} \frac{1}{N} \sum_{j=1}^N \left([p_{\tau_s}(j+n) - p_{\tau_s}(j)]^2 + [q_{\tau_s}(j+n) - q_{\tau_s}(j)]^2 \right) \tau_s^2 \,.$$

Similarly the power spectrum for the time-continuous case discretizes to

$$S(\nu) = \lim_{n \to \infty} \frac{1}{n} E \left| \sum_{j=0}^{n-1} e^{2\pi i \frac{\nu}{\nu_s} j} \phi(j) \right|^2 \tau_s^2, \tag{13}$$

where $\nu_s = 1/\tau_s$ is the sample frequency. For chaotic systems the power spectrum decays for large frequencies ν, and so for frequencies larger than some $\nu_{\max}$ the power spectrum is zero for all practical purposes.

Comparing (13) with the power spectrum (6) for discrete-time data, we identify

$$c = 2\pi \frac{\nu}{\nu_s}, \quad \nu \in [0, \nu_{\max}] . \tag{14}$$

Sampling at the Nyquist rate with $\nu_s^\star = 2\nu_{\max}$ corresponds to $c \in (0, \pi)$ as before. However, oversampling at a higher frequency $\nu_s > \nu_s^\star$, restricts the effective choices of c to $c \in (0, c^\star)$ where $c^\star = \frac{\nu_s^\star}{\nu_s} \pi < \pi$. In this case, the test for chaos may incorrectly classify the dynamics of a chaotic system as regular, since it is possible that more than half of the randomly chosen values of $c \in (0, \pi)$ will lie in $(c^\star, \pi)$ yielding a median $K = 0$. Note that the problem of oversampling is not related to the length N of the time series.

We illustrate this using the Rössler system (12) sampled with τ_s ranging from $\tau_s = 0.05$ up to $\tau_s = 1$. In Figure 15 the median of the asymptotic growth rate K is shown as a function of the sample time. For data that is too finely sampled, we obtain $K = 0$ although the dynamics is actually chaotic. Figure 16 illustrates how the range
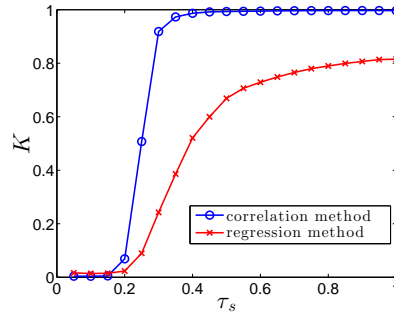
Fig. 15 Plot of K as a function of the sample time τ_s for the Rössler system (12). At the finest sampling rate $\tau_s = 0.05$ we recorded $N = 100,000$ data points. Results are shown for the correlation method (circles) and the regression method (crosses).

of effective values of c depends on the sampling time τ_s. The linear scaling of the range of c for which $K_c \approx 1$ as suggested by (14) is clearly seen. The pronounced dips of K_c for certain values of c are caused by near resonances which occur in the chaotic Rössler system for our parameter values caused by regularly appearing

revolutions of the dynamics as illustrated in Figure 13. Note that the presence of resonances does not affect the value of the median K as seen in Figure 15.
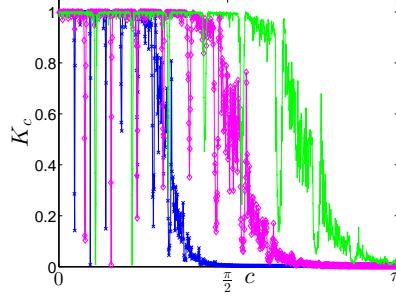
Fig. 16 Plot of K_c as a function of the frequency c for the Rössler system (12). From left to right we used $\tau_s = 0.15$, $\tau_s = 0.25$ and $\tau_s = 0.35$. The corresponding values of the growth rate (calculated using the correlation method) are $K = 0.005$, $K = 0.5$ and $K = 0.97$, respectively. At the sampling rate $\tau_s = 0.05$ we recorded $N = 100,000$ data points.

### 5.2.2 Partial differential equations

We apply now our test to the driven and damped nonlinear Schrödinger equation

$$\iota q_t + q_{xx} + 2|q|^2 q = -\iota \gamma q + \varepsilon e^{\iota(\omega t + \sigma)},$$

which describes a plasma resonantly driven by a capacitor with frequency ω and damped via collisions [57, 11, 4]. For $q = Q \exp(\iota(\omega t + \sigma))$ we solve

$$\iota Q_t + Q_{xx} + 2|Q|^2 Q = \omega Q - \iota \gamma Q + \varepsilon. \tag{15}$$

It is well known that for given system length L the system (15) undergoes a period doubling bifurcation route into chaos [57] for increasing values of the driving amplitude ε. We present here results for a system with length $L = 80$, $\gamma = 0.11$, $\omega = 1$ for $\varepsilon = 0.095$ and $\varepsilon = 0.2$ for regular and chaotic dynamics, respectively. The system (15) is integrated with a second-order in space and time finite difference Crank-Nicolson solver where the nonlinear term is treated with an Adams-Bashforth scheme. We use $n_x = 256$ grid points and an integration time step of $dt = 0.0001$ and evolve from an initial condition $q = -\iota\sqrt{2} + 0.1\cos(kx)$ with $k = 15$ with reflective (von Neumann) boundary conditions. In Figure 17 we show Hovmöller diagrams of $|Q(x,t)|$ for regular and chaotic dynamics. We construct observables by evaluating the field $Q(x,t)$ at spatial locations $x_j = jdx$ with $dx = L/n_x$ and $j = 1, \cdots, n_x$. In particular, we consider the following observables
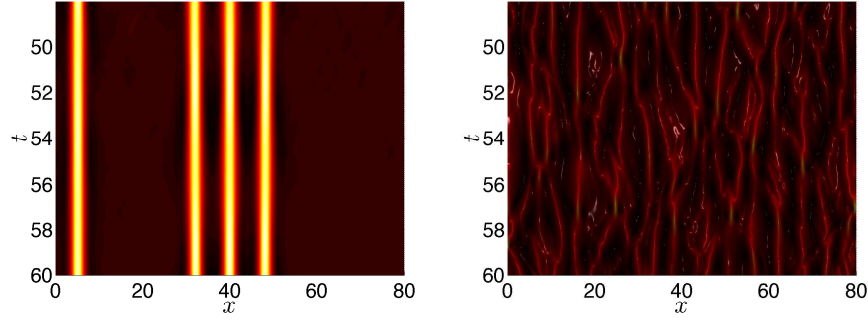
Fig. 17 Hovmöller diagram of $|Q(x,t)|$ for regular dynamics with $\varepsilon = 0.095$ (left) and chaotic dynamics with $\varepsilon = 0.2$ (right) for the driven and damped Schrödinger equation (15).

$$\phi_1(t) = \sum_{j=1}^{n_x} |Q(x_j,t)|,$$

$$\phi_2(t) = |Q(L/2,t)|,$$

$$\phi_3(t) = \sum_{j=1}^{5} |Q(x_{j^\star},t)|.$$

For the last observable $\phi_3(t)$ we randomly choose 5 locations $x_{j^\star}$ from the $n_x = 256$ spatial gridpoints at time $t = 0$.

The observables $\phi_{1,2,3}$ are sampled time every 0.3 time units with a total of 10,000 snapshots taken. This sampling time is sufficiently large to avoid the oversampling effects for continuous time systems which would lead to $K \approx 0$ irrespective of the underlying dynamics, as discussed in Section 5.2.1 (see also [22]). Using the correlation method on $D_c(n)$, for each of the three observables we obtain values of K smaller than 0.0017 in the regular case with $\varepsilon = 0.095$, and values of K within 0.003 from $K = 1$ for the chaotic case.

We note that although the nonlinear Schrödinger equation (15) is formally infinite-dimensional, its dynamics evolves on a finite dimensional attractor [11].

5.3 Data contaminated by noise

For a test for chaos to be able to analyse real world data one needs to show its capability to be able to process observations contaminated by noise. In the following we revisit the example of measurement noise in an 8-dimensional Lorenz-96 model studied in our previous work [20]. There it was shown that our 0-1 test for chaos is far superior to traditional methods using phase space reconstruction and Lyapunov exponents [66, 63], without preprocessing the data with standard noise reduction methods [31].

5.3.1 Lorenz-96 system

We revisit the tough test case of analysing quasi-periodic dynamics with measurement noise [20]. In particular we study the Lorenz-96 system [45]

$$\dot{z}_i = z_{i-1}(z_{i+1} - z_{i-2}) - z_i + F \qquad i = 1, \cdots, D \tag{16}$$

with periodic $z_{i+D} = z_i$. This system is a toy-model for midlatitude atmospheric dynamics, incorporating linear damping, forcing and nonlinear transport. In the atmospheric context one usually uses $D = 40$. This particular value for D is chosen such that the spacing between adjacent grid points z_i roughly equals the Rossby radius of deformation at midlatitudes where the circumference of the earth is roughly $30,000$ km. The dynamical properties of the Lorenz-96 system have been investigated, for example, in [46, 58]. We use $D = 8$ modes where quasi-periodic windows were found to alternate with chaotic dynamics [58].

In the previous examples, the test was able to distinguish sharply between regular and chaotic dynamics in noise free data. However such good performance of the test for noise free data is detrimental for noise contaminated data — even small amounts of noise would be detected and noisy regular dynamics would be falsely classified as chaotic. The sensitivity of our test was enhanced by the subtraction of the oscillatory term (cf. equation (4) and Figure 2), and the application of the correlation method. In [20] our test employed directly the mean square displacement $M_c(n)$ including the oscillatory term) rather than the modified version $D_c(n)$. Furthermore, it used the regression method rather than the correlation method to calculate K_c from the mean square displacement $M_c(n)$. We showed that in this case our test greatly outperforms methods involving phase space reconstruction and Lyapunov exponents in distinguishing quasi-periodic dynamics from chaotic dynamics when 10% measurement noise was added to the observations.

Here we will revisit our test including a method to deal with measurement noise proposed in [22]: If we assume that the noise is independent of the dynamics, i.e. pure measurement noise, and also independent of the forcing F, we can decompose the linear part of the modified mean square displacement as

$$D_c(n) = (S_{\text{dyn}}(c) + S_{\text{noise}}(c))n + o(n). \tag{17}$$

Here $S_{\text{dyn}}(c)$ is the variance associated with the underlying deterministic dynamics to be analysed and $S_{\text{noise}}(c)$ is the variance associated with the measurement noise. We can estimate the variance associated with the measurement noise $S_{\text{noise}}(c)$ by estimating $D_c(n)$ from the noisy observations at a parameter F where the dynamics is known to be regular with $S_{\text{dyn}}(c) = 0$. We then estimate $S_{\text{noise}}(c)$ to compensate for the linear growth of $D_c(n)$ due to the noise. We remark that this is not always possible and requires (at least) that gauge experiments can be performed. For example, this method cannot help with studying the regularity of planetary motion for noisy observations. If gauge experiments are not possible, our test can still be used to analyse noise-contaminated experimental data using the formulation proposed in

reference [20] as done, for example, in [13, 33, 34, 38, 37]. Once $S_{\text{noise}}(c)$ is estimated the test can proceed with

$$\hat{D}_c(n) = D_c(n) - S_{\text{noise}}(c)\,n \qquad (18)$$

as described in the previous sections. In particular we can employ the more sensitive correlation method. Note that the linear growth term of the mean-square displacement will not be entirely eliminated (unless by chance $S_{\text{noise}}(c)$ is correctly estimated from the data) but the proposed scheme controls its magnitude. This allows the test to analyse observational data of finite length; for unlimited noise-contaminated data, one would, of course, obtain $K = 1$, irrespective of the underlying deterministic dynamics.

In Figure 18 we show results of our test using first $M_c(n)$ and the regression method as in [20] and second using $\hat{D}_c(n)$ and the correlation method. We use a fourth-order Runge-Kutta scheme with a time step of $dt = 0.05$ to generate observations

$$\phi(t) = (1 + \zeta)(z_2 + z_3 + z_4). \qquad (19)$$

The measurement noise $\zeta = \eta u$ is drawn from a uniform distribution $u \sim \mathscr{U}[-1, 1]$. In Figure 18 we show results for noise-free observations with $\eta = 0$, and for measurement noise levels of 10% and 20% with $\eta = 0.1$ and $\eta = 0.2$, respectively. Observations are taken every 2.5 time units and a total of $N = 100,000$ observations are taken.

We gauge the variance due to the noise at $F = 5.25$. We obtain $S_{\text{noise}} = 0.3$ and $S_{\text{noise}} = 0.62$ for a noise level η of 10% and 20% observational noise, respectively. Both methods detect the quasi-periodic windows well for 10% measurement noise (we remark that methods relying on phase space reconstruction and maximal Lyapunov exponents were not able to accurately distinguish quasi-periodic dynamics from chaotic dynamics [20]). The distinction between quasi-periodic dynamics and chaotic dynamics with a noise level of 20% is less clear in the test employing $M_c(n)$ but still remarkably good when using $\hat{D}_c(n)$. We propose this example which involves noise contaminated quasi-periodic dynamics as a challenge for other tests.

6 Summary

We have described the 0–1 test for chaos, focusing on its implementation and several practical issues as well as on the theoretical justifications outlining the realm of validity of the test. We have illustrated the versatility and efficiency of our method by treating the notoriously difficult case of weakly chaotic separatrix layers in the standard map as well as analysing measurement noise contaminated data.

The advantage of our method lies in a) its computational low cost and ease of implementation, b) its generality of applicability independent of the nature of the dynamical system and its dimension, c) its working directly with the time series without the need for phase space reconstruction, d) its ability to detect weak chaos
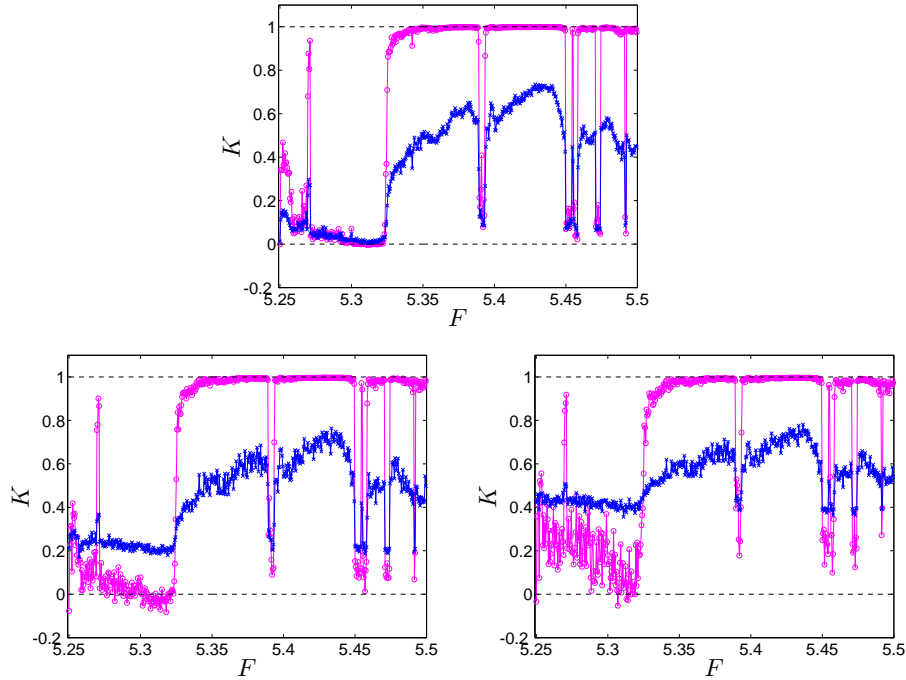
Fig. 18 Plot of K versus F for the Lorenz-96 system (16) for $5.25 \leq F \leq 5.5$ increased in increments of 0.005. We used $N = 100,000$ data points sampled at 2.5 time units. Top: Noise free data; Bottom left: 10% measurement noise; Bottom right: 20% measurement noise. K is calculated via the regression method for $M_c(n)$ (crosses, blue) and for the correlation method for $D_c(n)$ with subtracted noise variance (circles, magenta). The horizontal lines indicate the limiting cases $K = 0$ and $K = 1$. We used 100 randomly distributed values of c.

and e) its ability to detect regular behaviour within noisy data. In particular, we mention the 8-dimensional Lorenz-96 model contaminated by noise (see Section 5.3). We are not aware of any other method that comes close to matching the effectiveness of our test for this example.

The theoretical justification of the 0-1 test depends on the nature of attractors for general smooth (or piecewise smooth) dynamical systems. In [23] we challenged the skeptical reader to construct a robust smooth example where the test fails. So far, no such example has come to light. This was explored further in [26] where we formulated a conjecture which, roughly speaking, states that for typical smooth dynamics, either $K_c = 1$ for almost every c or $K_c = 0$ for almost every c.

References

[1] Ashwin, P., Melbourne, I., and Nicol, M. (2001). Hypermeander of spirals; local bifurcations and statistical properties. *Physica D*, **156**, 364–382.

[2] Bernardini, D., Rega, G., Litak, G., and Syta, A. (2013). Identification of regular and chaotic isothermal trajectories of a shape memory oscillator using the 0–1 test. *Proceedings of the Institution of Mechanical Engineers, Part K: Journal of Multi-body Dynamics*, **227**(1), 17–22.

[3] Cafagna, D. and Grassi, G. (2010). An effective method for detecting chaos in fractional-order systems. *International Journal of Bifurcation and Chaos*, **20**(03), 669–678.

[4] Cai, D. and McLaughlin, D. W. (2000). Chaotic and turbulent behaviour of unstable one-dimensional nonlinear dispersive waves. *Journal of Mathematical Physics*, **41**(6), 4125–4153.

[5] Cao, J., Syta, A., Litak, G., Zhou, S., Inman, D., and Chen, Y. (2015). Regular and chaotic vibration in a piezoelectric energy harvester with fractional damping. *The European Physical Journal Plus*, **130**(6).

[6] Chirikov, B. V. (1979). A universal instability of many-dimensional oscillator systems. *Phys. Rep.*, **52**, 263.

[7] Chowdhury, D. R., Iyengar, A. N. S., and Lahiri, S. (2012). Gottwald Melborune (0–1) test for chaos in a plasma. *Nonlinear Processes in Geophysics*, **19**(1), 53–56.

[8] Dafilis, M., Frascoli, F., McVernon, J., Heffernan, J. M., and McCaw, J. M. (2014a). The dynamical consequences of seasonal forcing, immune boosting and demographic change in a model of disease transmission. *Journal of Theoretical Biology*, **361**, 124–132.

[9] Dafilis, M., Frascoli, F., McVernon, J., Heffernan, J., and McCaw, J. (2014b). Dynamical crises, multistability and the influence of the duration of immunity in a seasonally-forced model of disease transmission. *Theoretical Biology and Medical Modelling*, **11**(1), 43.

[10] Diddens, C. and Linz, S. J. (2013). Continuum modeling of particle redeposition during ion-beam erosion. *The European Physical Journal B*, **86**(9), 1–13.

[11] Eickermann, T., Grauer, R., and Spatschek, K. H. (1995). Identification of mass capturing structures in a perturbed nonlinear Schrödinger equation. *Physics Letters A*, **198**, 383–388.

[12] Erzgräber, H., Wieczorek, S., and Krauskopf, B. (2010). Dynamics of two semiconductor lasers coupled by a passive resonator. *Phys. Rev. E*, **81**, 056201.

[13] Falconer, I., Gottwald, G. A., Melbourne, I., and Wormnes, K. (2007). Application of the 0–1 Test for chaos to experimental data. *SIAM J. Appl. Dyn.*, **6**, 395–402.

[14] Field, M., Melbourne, I., and Török, A. (2003). Decay of correlations, central limit theorems and approximation by Brownian motion for compact Lie group extensions. *Ergodic Theory Dyn. Syst.*, **23**, 87–110.

[15] Field, M., Melbourne, I., and Török, A. (2005). Stable ergodicity for smooth compact Lie group extensions of hyperbolic basic sets. *Ergodic Theory Dyn. Syst.*, **25**, 517–551.

[16] Fraser, A. M. and Swinney, H. L. (1986). Independent coordinates for strange attractors from mutual information. *Phys. Rev. A*, **33**, 1134–1140.

[17] Gaspard, P. and Wang, X.-J. (1988). Sporadicity: Between periodic and chaotic dynamical behaviours. *Proceedings of the National Academy of Sciences*, **85**, 4591–4595.

[18] Gopal, R., Venkatesan, A., and Lakshmanan, M. (2013). Applicability of 0-1 test for strange nonchaotic attractors. *Chaos: An Interdisciplinary Journal of Nonlinear Science*, **23**(2), 023123.

[19] Gottwald, G. A. and Melbourne, I. (2004). A new test for chaos in deterministic systems. *Proc. Roy. Soc. A*, **460**, 603–611.

[20] Gottwald, G. A. and Melbourne, I. (2005). Testing for chaos in deterministic systems with noise. *Physica D*, **212**(1-2), 100–110.

[21] Gottwald, G. A. and Melbourne, I. (2008). Comment on "Reliability of the 0–1 test for chaos". *Phys. Rev. E*, **77**, 028201.

[22] Gottwald, G. A. and Melbourne, I. (2009a). On the implementation of the 0–1 test for chaos. *SIAM J. Appl. Dyn.*, **8**, 129–145.

[23] Gottwald, G. A. and Melbourne, I. (2009b). On the validity of the 0–1 test for chaos. *Nonlinearity*, **22**, 1367–1382.

[24] Gottwald, G. A. and Melbourne, I. (2013a). A Huygens principle for diffusion and anomalous diffusion in spatially extended systems. *Proc. Natl. Acad. Sci. USA*, **110**, 8411–8416.

[25] Gottwald, G. A. and Melbourne, I. (2013b). Central limit theorems and suppression of anomalous diffusion for systems with symmetry. *submitted*.

[26] Gottwald, G. A. and Melbourne, I. (2014). A test for a conjecture on the nature of attractors for smooth dynamical systems. *Chaos*, **24**, 024403.

[27] Gouëzel, S. (2004). Central limit theorem and stable laws for intermittent maps. *Probability Theory and Related Fields*, **128**, 82–122.

[28] He, K., Xu, Y., Zou, Y., and Tang, L. (2015). Electricity price forecasts using a curvelet denoising based approach. *Physica A: Statistical Mechanics and its Applications*, pages –.

[29] Howard, J. (2005). Discrete virial theorem. *Celestial Mechanics and Dynamical Astronomy*, **92**(1-3), 219–241.

[30] Hu, H. (2004). Decay of correlations for piecewise smooth maps with indifferent fixed points. *Ergodic Theory Dynam. Systems*, **24**, 495–524.

[31] Kantz, H. and Schreiber, T. (1997). *Nonlinear Time Series Analysis*. Cambridge University Press, Cambridge.

[32] Kędra, M. (2014). Deterministic chaotic dynamics of Raba River flow (Polish Carpathian Mountains). *Journal of Hydrology*, **509**, 474 – 503.

[33] Krese, B. and Govekar, E. (2012). Nonlinear analysis of laser droplet generation by means of 0–1 test for chaos. *Nonlinear Dynamics*, **67**, 2101–2109.

[34] Krese, B. and Govekar, E. (2013). Analysis of traffic dynamics on a ring road-based transportation network by means of 0–1 test for chaos and Lyapunov spectrum. *Transportation Research Part C: Emerging Technologies*, **36**, 27 – 34.

[35] Kulp, C. W. and Smith, S. (2011). Characterization of noisy symbolic time series. *Phys. Rev. E*, **83**, 026201.

[36] Kříž, R. (2013). Chaotic analysis of the GDP time series. In I. Zelinka, G. Chen, O. E. Rössler, V. Snasel, and A. Abraham, editors, *Nostradamus 2013: Prediction, Modeling and Analysis of Complex Systems*, volume 210 of *Advances in Intelligent Systems and Computing*, pages 353–362. Springer International Publishing.

[37] Kříž, R. (2014). Finding chaos in finnish gdp. *International Journal of Automation and Computing*, **11**(3), 231–240.

[38] Kříž, R. and Kratochvĭl, Š. (2014). Analyses of the chaotic behavior of the electricity price series. In A. Sanayei, I. Zelinka, and O. E. Rössler, editors, *ISCS 2013: Interdisciplinary Symposium on Complex Systems*, volume 8 of *Emergence, Complexity and Computation*, pages 215–226. Springer Berlin Heidelberg.

[39] Leon, F. (2014). Design and evaluation of a multiagent interaction protocol generating behaviours with different levels of complexity. *Neurocomputing*, **146**, 173–186.

[40] Li, X., Gao, G., Hu, T., Ma, H., and Li, T. (2015). Multiple time scales analysis of runoff series based on the chaos theory. *Desalination and Water Treatment*, **52**(13-15), 2741–2749.

[41] Lichtenberg, A. and Lieberman, M. (1992). *Regular and chaotic dynamics*. Applied mathematical sciences. Springer-Verlag.

[42] Litak, G. and Syta, A. andWiercigroch, M. (2009). Identification of chaos in a cutting process by the 0-1 test. *Chaos, Solitons & Fractals*, **40**, 2095–2101.

[43] Litak, G., Radons, G., and Schubert, S. (2009). Identification of chaos in a regenerative cutting process by the 0-1 test. *Proc. Appl. Math. Mech.*, **9**(1), 299–300.

[44] Liverani, C., Saussol, B., and Vaienti, S. (1999). A probabilistic approach to intermittency. *Ergodic Theory Dynam. Systems*, **19**, 671–685.

[45] Lorenz, E. N. (1996). Predictability - a problem partly solved. In T. Palmer, editor, *Predictability*. European Centre for Medium-Range Weather Forecast, Shinfield Park, Reading, UK.

[46] Lorenz, E. N. and Emanuel, K. A. (1998). Optimal sites for supplementary weather observations: simulation with a small model. *Journal of the Atmospheric Sciences*, **55**(3), 399–414.

[47] Lugo-Fernández, A. (2007). Is the loop current a chaotic oscillator? *Journal of Physical Oceanography*, **37**(6), 1455–1469.

[48] Martinsen-Burrell, N., Julien, K., Petersen, M. R., and Weiss, J. B. (2006). Merger and alignment in a reduced model for three-dimensional quasi-geostrophic ellipsoidal vortices. *Phys. Fluids*, **18**, 057101.

[49] MATLAB (2010). *version 7.10.0 (R2010a)*. The MathWorks Inc., Natick, Massachusetts.

[50] McLennan-Smith, T. A. and Mercer, G. N. (2014). Complex behaviour in a dengue model with a seasonally varying vector population. *Mathematical Biosciences*, **248**(0), 22 – 30.

[51] Melbourne, I. and Gottwald, G. A. (2008). Power spectra for deterministic chaotic dynamical systems. *Nonlinearity*, **21**, 179–189.

[52] Melbourne, I. and Nicol, M. (2004). Statistical properties of endomorphisms and compact group extensions. *J. London. Math. Soc.*, **70**, 427–446.

[53] Melbourne, I. and Török, A. (2004). Statistical limit theorems for suspension flows. *Israel Journal of Math.*, **144**, 191–209.

[54] Melbourne, I. and Zweimüller, R. (2015). Weak convergence to stable Lévy processes for nonuniformly hyperbolic dynamical systems. *Ann. Inst. H. Poincaré (B) Probab. Stat.*, **51**, 545–556.

[55] Nair, V. and Sujith, R. (2015). A reduced-order model for the onset of combustion instability: Physical mechanisms for intermittency and precursors. *Proceedings of the Combustion Institute*, **35**(3), 3193–3200.

[56] Nicol, M., Melbourne, I., and Ashwin, P. (2001). Euclidean extensions for dynamical systems. *Nonlinearity*, **14**, 275–300.

[57] Nozaki, K. and Bekki, N. (1986). Low-dimensional chaos in a driven damped nonlinear Schrödinger equation. *Physica D*, **21**, 381–393.

[58] Orrell, D. and Smith, L. (2003). Visualising bifurcations in high dimensional systems: The spectral bifurcation diagram. *International Journal of Bifurcation and Chaos*, **13**(10), 3015–3028.

[59] Pomeau, Y. and Manneville, P. (1980). Intermittent transition to turbulence in dissipative dynamical systems. *Comm. Math. Phys.*, **74**, 189–197.

[60] Prabin Devi, S., Singh, S. B., and Surjalal Sharma, A. (2013). Deterministic dynamics of the magnetosphere: results of the 0-1 test. *Nonlinear Processes in Geophysics*, **20**(1), 11–18.

[61] Press, W. H., Teukolsky, S. A., Vetterling, W. T., and Flannery, B. P. (2007). *Numerical Recipes 3rd Edition: The Art of Scientific Computing*. Cambridge University Press, New York, NY, USA, 3 edition.

[62] Radons, G. and Zienert, A. (2013). Nonlinear dynamics of complex hysteretic systems: Oscillator in a magnetic field. *The European Physical Journal Special Topics*, **222**(7), 1675–1684.

[63] Rosenstein, M. T., Collins, J. J., and De Luca, C. J. (1993). A practical method for calculating largest Lyapunov exponents from small data sets. *Physica D*, **65**, 117–134.

[64] Rössler, O. (1976). An equation for continuous chaos. *Physics Letters A*, **57**(5), 397 – 398.

[65] Swathy, P. S. and Thamilmaran, K. (2014). Dynamics of SC-CNN based variant of MLC circuit: An experimental study. *International Journal of Bifurcation and Chaos*, **24**(02), 1430008.

[66] Takens, F. (1981). Detecting strange attractors in turbulence. In *Dynamical systems and turbulence, Warwick 1980 (Coventry 1979/1980)*, volume 898 of *Lecture Notes in Math.*, pages 366–381. Springer, Berlin.

[67] Tsai, T.-L. and Dawes, J. H. (2013). Dynamics near a periodically-perturbed robust heteroclinic cycle. *Physica D: Nonlinear Phenomena*, **262**, 14–34.

[68] Webel, K. (2012). Chaos in German stock returns - New evidence from the 0–1 test. *Economics Letters*, **115**(3), 487 – 489.

[69] Xin, B. and Li, Y. (2013). 0-1 test for chaos in a fractional order financial system with investment incentive. *Abstract and Applied Analysis*, **2013**, 876298.

[70] Xin, B. and Zhang, J. (2015). Finite-time stabilizing a fractional-order chaotic financial system with market confidence. *Nonlinear Dynamics*, **79**(2), 1399–1409.

[71] Yuan, L., Yang, Q., and Zeng, C. (2013). Chaos detection and parameter identification in fractional-order chaotic systems with delay. *Nonlinear Dynamics*, **73**(1-2), 439–448.

[72] Zachilas, L. and Psarianos, I. N. (2012). Examining the chaotic behavior in dynamical systems by means of the 0–1 test. *Journal of Applied Mathematics*, **2012**, 681296.

[73] Zaslavskii, G. M., Sagdeev, R. Z., Usikov, D. A., Chernikov, A. A., and Sagdeev, A. R. (1992). *Chaos and Quasi-Regular Patterns*. Cambridge University Press, Cambridge.

[74] Zweimüller, R. (2003). Stable limits for probability preserving maps with indifferent fixed points. *Stoch. Dyn.*, **3**, 83–99.